Holographic x-ray image reconstruction through the application of differential and integral operators

Manuel Guizar-Sicairos,[1],* Diling Zhu,[2,3] James R. Fienup,[1] Benny Wu,[2,3] Andreas Scherz,[3] and Joachim Stöhr[3,4]

[1]*The Institute of Optics, University of Rochester, Rochester, New York 14627, USA*
[2]*Department of Applied Physics, Stanford University, Stanford, California 94305, USA*
[3]*Stanford Institute for Materials and Energy Science, Menlo Park, California 94025, USA*
[4]*Linac Coherent Light Source, SLAC National Accelerator Laboratory, Menlo Park, California 94025, USA*
*Corresponding author: mguizar@optics.rochester.edu

We introduce a noniterative image-reconstruction technique for coherent diffractive imaging. Through the application of differential and integral operators, an extended reference can be used to recover the complex-valued transmissivity of an object, in closed form, from a measurement of its far-field (Fraunhofer) diffraction intensity. We demonstrate the feasibility of this approach, using a reference of a pair of crossed wires and slits, through numerical simulations and a soft x-ray coherent diffractive imaging experiment. © 2010 Optical Society of America

OCIS codes: 090.0090, 100.3200, 100.3010, 180.7460.

Reconstructing the transmissivity of a sample from its Fraunhofer diffraction intensity (coherent diffractive imaging) has important applications for high-resolution imaging at x-ray and optical wavelengths, ranging from integrated circuit inspection to solid-state physics and biology. Upon measurement, the phase of the coherent field is lost and must be computationally recovered to obtain a reconstructed image. Although this problem can be solved by iterative transform algorithms if the intensity measurement is adequately sampled [1,2], this approach is computationally expensive and may suffer from stagnation and/or ambiguity problems.

Holographic techniques can alleviate this computational burden and obtain a reconstruction in a noniterative computation. X-ray Fourier transform holography (FTH) has been implemented by including a point reference in the vicinity of the object [3,4]. The phase of the object field is then encoded in the interference of the object and reference waves, thus allowing a closed-form reconstruction. The resolution for this approach is, however, limited by the size of the point reference.

In this Letter we introduce a noniterative technique that allows direct and unique image reconstruction through the application of differential and integral operators. This approach generalizes the holographic method in [5] and allows a more general class of extended reference structures. In particular it allows a pair of crossed wires (or slits) to be used as a reference, where the object phase is encoded through its interference with light diffracted from the wires' overlap region. This can improve the resolution beyond FTH because of the availability of thin-wire structures such as carbon nanotubes [6].

Assume the field transmitted through the object plane can be expressed as the sum of an object additive modulation, $o(x,y)$, and a reference, $r(x,y)$, i.e. $f(x,y) = o(x,y) + r(x,y)$. The inverse Fourier transform (FT) of the measured Fourier intensity is the field autocorrelation, given by

$$f \otimes f = o \otimes o + r \otimes r + o \otimes r + r \otimes o, \quad (1)$$

where $\otimes$ denotes cross correlation. If $r(x,y)$ satisfies

$$\mathcal{L}^{(n)}\{r(x,y)\} = A\mathcal{D}^{(m)}\{d(x - x_0, y - y_0)\} + g(x,y), \quad (2)$$

where $d(x,y)$ is a delta-like function, A is a complex-valued constant, $g(x,y)$ allows for additional terms, and $\mathcal{L}^{(n)}\{\cdot\}$ and $\mathcal{D}^{(m)}\{\cdot\}$ are linear differential operators of order n and m, respectively. Then it can be shown that

$$\begin{aligned}
\mathcal{L}^{(n)}\{f \otimes f\} = {} & \mathcal{L}^{(n)}\{o \otimes o\} + \mathcal{L}^{(n)}\{r \otimes r\} \\
& + (-1)^n o \otimes g + g \otimes o + (-1)^n A^* \\
& \times \mathcal{D}^{(m)}\{o(x + x_0, y + y_0) * d^*(-x, -y)\} \\
& + A\mathcal{D}^{(m)}\{o^*(x_0 - x, y_0 - y) * d(x,y)\}, \quad (3)
\end{aligned}$$

where $*$ denotes convolution. We can then directly extract $\mathcal{D}^{(m)}\{o(x + x_0, y + y_0) * d^*(-x, -y)\}$, provided it does not overlap with other terms, and recover the object by computing $\mathcal{D}^{(-m)}\{\cdot\}$, i.e., an integral operator. The effects of missing information in the Fourier domain and separation conditions can be derived in a manner analogous to that in [5].

Notice that the reconstruction, $o(x + x_0, y + y_0)$, will be convolved with $d^*(-x, -y)$. The resolution of the reconstruction is then limited by the size of $d(x,y)$ or by $\Delta x = \lambda z / D$ (in the paraxial approximation), whichever is larger. In the latter, λ is the illumination wavelength and z is the distance from the object to a detector of diameter D. In practice the resolution can be worse if the measurement has a poor signal-to-noise ratio (SNR).

Let us now apply this formulation to the specific case of a crossed-wires reference, with individual

wire width w and transmissivity B. If the wires extend well beyond the object, the transmissivity of $r(x,y)$ is given by

$$r(x+x_0,y+y_0) = 1 - (1-B)\left[\text{rect}\left(\frac{y\cos\alpha - x\sin\alpha}{w}\right)\right.$$
$$\left. + \text{rect}\left(\frac{y\cos\beta - x\sin\beta}{w}\right)\right] + Ad(x,y),$$

$$(4)$$

where the individual wires make angles α and β with respect to the x axis ($\alpha \neq \beta$) as shown in Fig. 1, rect($\cdot$) is the rectangle function, and

$$Ad(x,y) = (1-B)^2 \text{rect}\left(\frac{y\cos\alpha - x\sin\alpha}{w}\right)$$
$$\times \text{rect}\left(\frac{y\cos\beta - x\sin\beta}{w}\right) \qquad (5)$$

is the overlap region of the two wires.

It follows from Eq. (4) that $[\hat{\alpha}\cdot\nabla][\hat{\beta}\cdot\nabla]r(x,y) = A[\hat{\alpha}\cdot\nabla][\hat{\beta}\cdot\nabla]d(x-x_0,y-y_0)$. So this reference satisfies Eq. (2) with $\mathcal{L}^{(2)}\{\cdot\} = \mathcal{D}^{(2)}\{\cdot\} = [\hat{\alpha}\cdot\nabla][\hat{\beta}\cdot\nabla]$ and $g(x,y) = 0$. In this case $\mathcal{D}^{(-2)}\{\cdot\} = \mathcal{L}^{(-2)}\{\cdot\}$, which consists of two line integrals in the direction of $\hat{\alpha}$ and $\hat{\beta}$, respectively. Since $\mathcal{L}^{(2)}\{r\otimes r\} = |A|^2\mathcal{L}^{(2)}\{d\otimes d\}$, the only separation condition of concern is from the term $\mathcal{L}^{(2)}\{o\otimes o\}$, which is analogous to the separation condition for the point reference in FTH. Because the object and reference overlap, $o(x,y) \propto t(x,y)-1$ [5].

A numerically simulated field, containing the object of interest and a crossed-wires reference ($B=0$), is shown in Fig. 2(a). The measured intensity was simulated by taking the FT of this field and computing its squared modulus. The field autocorrelation, $f\otimes f$, obtained by computing the inverse FT of the simulated intensity, is shown in Fig. 2(b).

Notice that the net effect of applying $\mathcal{L}^{(-2)}\{\mathcal{L}^{(2)}\{o\otimes r\}\}$ is to remove any function that is constant along the direction of the wires. The same effect can be obtained, with a more convenient processing, by directly estimating and removing these functions. First, we extract from the autocorrelation an $M\times N$ pixel region, $a_{m,n}$, that contains the reconstruction.
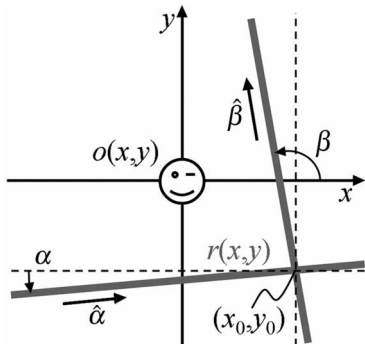
Fig. 1. Object with crossed-wires reference.
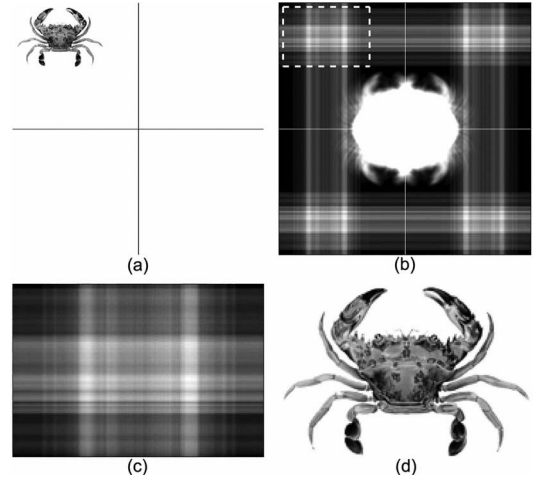
Fig. 2. (a) 512×512 object space field amplitude, $f(x,y)$. (b) Field autocorrelation, $f\otimes f$; an overall bias was subtracted for better visualization. (c) Cross correlation of object and crossed wires extracted from (b). (d) Object transmissivity reconstructed from (c).

This region is indicated by a dashed rectangle in Fig. 2(b) and shown in Fig. 2(c). An intermediate function, $b_{m,n}$, is obtained by subtracting, from each column, the average value of its first and last element,

$$b_{m,n} = a_{m,n} - (a_{1,n} + a_{M,n})/2. \qquad (6)$$

We repeat the procedure for all the rows to arrive at a reconstruction of the object

$$o_{m,n} = b_{m,n} - (b_{m,1} + b_{m,N})/2. \qquad (7)$$

This procedure removes the functions that are constant along the direction of the wires for $\alpha=0$ and $\beta=90°$, and gives a direct reconstruction. Combined with autocorrelation rotation(s), reconstructions can be obtained from crossed wires at arbitrary angles. Figure 2(d) shows the reconstructed transmissivity, $t(x,y) = o(x,y) + 1$.

A proof of concept experiment was performed at the soft x-ray coherent scattering beam line of the Stanford Synchrotron Radiation Lightsource (SSRL). The object [7] and a crossed-slits reference were fabricated using a focused ion beam on a 200 nm gold film supported by an Si_3N_4 membrane, as shown in Figs. 3(a) and 3(b). The mathematical formulation as described above holds for either crossed wires or crossed slits with slight modifications to Eqs. (4) and (5). In particular, in Eq. (5), $(1-B)^2$ should be replaced by $(B-1)$, where B is now the substrate transmissivity. Also, for this case $o(x,y) \propto t(x,y) - B$.

The sample was illuminated with a 650 eV ($\lambda \approx 1.9$ nm) spatially coherent x-ray beam [8]. The 1024×1024 diffraction pattern, shown in Fig. 3(a), was obtained by summing multiple exposures (cumulative exposure of 100 s) from a 16-bit, back-illuminated CCD with 20×20 micrometer pixels, placed 150 mm from the sample and using a 1.1 mm diameter beam stop.

After rotating the diffraction pattern (with interpolation) and smoothing out the beam stop edge, we computed an inverse FT and obtained the field auto-
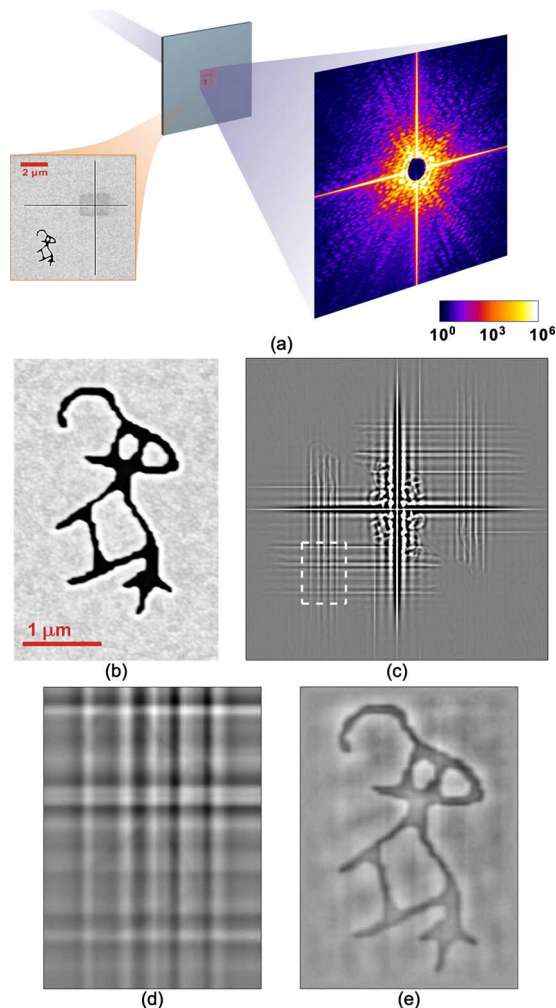
Fig. 3. (Color online) (a) Experimental setup and measured diffraction pattern (600×600 inset, number of photons, logarithmic scale). (b) SEM image of the sample. (c) Autocorrelation computed from an inverse FT of the measured data. (d) Region extracted from (c). (e) Direct reconstruction from (d). Real part is shown in (c), (d), and (e).

correlation shown in Fig. 3(c). We then extracted the pixel area shown in Fig. 3(d), which corresponds to the reconstruction. Because the transmissivity of the slits was not constant, strong streak artifacts were observed upon reconstruction if only a constant term was removed from each row and column.

To mitigate this, we used five pixels around the edge of Fig. 3(d) to estimate a linear function, for each column and row, through a closed-form linear least-squares fit. These functions were then removed to arrive at the reconstruction shown in Fig. 3(e), which compares favorably to the SEM in Fig. 3(b). The reconstruction is high-pass filtered because of the loss of the low spatial frequency data, due to the beam stop. The resolution (~ 30 nm) was set by the width of the slits.

We have introduced and demonstrated a novel, noniterative method to uniquely reconstruct the complex-valued transmissivity of an object, from a far-field intensity measurement, through the application of differential and integral operators. This generalizes the closed-form holographic method in [5] to a broader class of complex-valued extended references beyond those in [5,9–11].

This formulation allows the use of a pair of crossed wires or slits (amplitude and/or phase) as an extended reference. The reconstruction is then obtained, in closed form, from the cross correlation of the object and the overlap function, $d(x, y)$. Although the mathematical derivation is more straightforward using differential and integral operators, for this reference it is more convenient to directly remove functions that are constant along the direction of the wires outside of the object support. Unlike a deconvolution approach [12], all parameters relevant to the reconstruction can be estimated directly from the data, with no *a priori* quantitative information about the sample required. We have shown that this approach is robust to missing information due to a beam stop.

References

1. J. R. Fienup, Appl. Opt. **21**, 2758 (1982).
2. J. Miao, P. Charalambous, J. Kirz, and D. Sayre, Nature **400**, 342 (1999).
3. I. McNulty, J. Kirz, C. Jacobsen, E. H. Anderson, M. R. Howells, and D. P. Kern, Science **256**, 1009 (1992).
4. S. Eisebitt, J. Lüning, W. F. Schlotter, M. Lörgen, O. Hellwig, W. Eberhardt, and J. Stöhr, Nature **432**, 885 (2004).
5. M. Guizar-Sicairos and J. R. Fienup, Opt. Express **15**, 17592 (2007).
6. X. Zhao, Y. Liu, S. Inoue, T. Suzuki, R. O. Jones, and Y. Ando, Phys. Rev. Lett. **92**, 125502 (2004).
7. Ancient Chinese character "elephant," which later inherited the meaning of "image" from their phonetic connection, http://en.wikipedia.org/wiki/Oracle_bone_script.
8. R. Rick, A. Scherz, W. F. Schlotter, D. Zhu, J. Lüning, and J. Stöhr, Opt. Lett. **34**, 650 (2009).
9. S. G. Podorov, K. M. Pavlov, and D. M. Paganin, Opt. Express **15**, 9954 (2007).
10. M. Guizar-Sicairos and J. R. Fienup, Opt. Lett. **33**, 2668 (2008).
11. B. Enders, K. Giewekemeyer, T. Kurz, S. Podorov, and T. Salditt, New J. Phys. **11**, 043021 (2009).
12. H. He, U. Weierstall, J. C. H. Spence, M. Howells, H. A. Padmore, S. Marchesini, and H. N. Chapman, Appl. Phys. Lett. **85**, 2454 (2004).